Published in final edited form as:
Cell. 2012 August 3; 150(3): 620–632. doi:10.1016/j.cell.2012.06.027.

Brown Remodeling of White Adipose Tissue by SirT1-Dependent Deacetylation of Pparγ

Li Qiang[1], **Liheng Wang**[1,*], **Ning Kon**[2,*], **Wenhui Zhao**[2], **Sangkyu Lee**[4], **Yiying Zhang**[3], **Michael Rosenbaum**[3], **Yingming Zhao**[4], **Wei Gu**[2], **Stephen R. Farmer**[5], and **Domenico Accili**[1]

[1]Naomi Berrie Diabetes Center, Department of Medicine, College of Physicians & Surgeons of Columbia University, New York, NY 10032

[2]Institute of Cancer Genetics, Department of Pathology, College of Physicians & Surgeons of Columbia University, New York, NY 10032

[3]Division of Molecular Genetics, Department of Pediatrics, College of Physicians & Surgeons of Columbia University, New York, NY 10032

[4]Ben May Department for Cancer Research, University of Chicago, Chicago, Illinois 60637, USA

[5]Department of Biochemistry, Boston University School of Medicine, Boston, Massachusetts 02118, US

SUMMARY

Brown adipose tissue (BAT) can disperse stored energy as heat. Promoting BAT-like features in white adipose (WAT) is an attractive, if elusive therapeutic approach to staunch the current obesity epidemic. Here we report that gain-of-function of the NAD-dependent deacetylase SirT1 or loss-of-function of its endogenous inhibitor Deleted in breast cancer-1 (Dbc1) promote "browning" of WAT by deacetylating peroxisome proliferator-activated receptor (Ppar)-γ on Lys268 and Lys293. SirT1-dependent deacetylation of Lys268 and Lys293 is required to recruit the BAT program coactivator Prdm16 to Pparγ, leading to selective induction of BAT genes and repression of visceral WAT genes associated with insulin resistance. An acetylation-defective Pparγ mutant induces a brown phenotype in white adipocytes, while an acetylated mimetic fails to induce "brown" genes, but retains the ability to activate "white" genes. We propose that SirT1-dependent Pparγ deacetylation is a form of selective Pparγ modulation of potential therapeutic import.

INTRODUCTION

Obesity and its comorbidities pose a growing therapeutic challenge (Wang et al., 2011). White adipose tissue (WAT) is the main 'storage site' of excess energy, primarily in the form of triglycerides. In addition, a functionally and morphologically distinct adipocyte subset–whose dense mitochondrial, innervation and vascular content earned it the moniker of 'brown' adipose tissue (BAT)–dissipates energy as heat (non-shivering thermogenesis).

Correspondence to: Domenico Accili (da230@columbia.edu).
*Equal contributors

Brown adipocytes uncouple mitochondrial electron transport from ATP synthesis to a greater extent than other cells by permeabilizing the inner mitochondrial membrane to allow inter-membrane proton to leak back into the mitochondrial matrix, primarily through uncoupling protein-1 (Ucp1), but also through other mitochondrial proteins (Ravussin and Galgani, 2011). Promoting BAT function has therapeutic potential to combat obesity (Farmer, 2009). But its limited amount and activity in humans are unlikely to offset the positive energy balance associated with excessive WAT deposition (Virtanen and Nuutila, 2011).

As an alternative strategy to increase energy expenditure and prevent weight gain, we investigated mechanisms that confer BAT-like features onto WAT, thus remodeling the latter from an energy-storage into an energy-disposal site (Kozak, 2010). The metabolic benefits of this conversion include prevention of diet-induced obesity and increased insulin sensitivity (Seale et al., 2011). Browning of rodent WAT can be brought about by hormones and cytokines, such as Irisin (Bostrom et al., 2012) and Fgf21 (Fisher et al., 2012), as well as by transcriptional modulation through Prdm16 (Seale et al., 2011), FoxC2 (Cederberg et al., 2001), RIP140 (Powelka et al., 2006), 4E-BP1 (Tsukiyama-Kohara et al., 2001), TIF2 (Picard et al., 2002), pRb and p107 (Scime et al., 2005). However, there is an unmet need for strategies that would translate these mechanisms into the clinic.

Activation of the nuclear receptor Pparγ by thiazolidinediones (TZDs) can also induce a brown-like phenotype in white adipocytes by promoting expression of brown adipocyte-specific genes (brown genes) and suppressing visceral WAT genes (white genes) (Vernochet et al., 2009). The mechanism of this ‘browning’ effect is unclear, and is unlikely to be clinically applicable without further modulation, in view of the adverse effects associated with TZD use (Kim-Muller and Accili, 2011).

Activation of the NAD^+-dependent deacetylase SirT1 by small molecules, calorie restriction or exercise promotes mitochondrial biogenesis and activities (Canto et al., 2009; Milne et al., 2007), raising the possibility that SirT1 regulates BAT functions. Furthermore, SirT1 gain-of-function mimics the insulin-sensitizing function of Pparγ ligands *in vivo* (Banks et al., 2008). In view of these facts, we asked whether the browning activity of Pparγ is mediated through its SirT1-dependent deacetylation and whether SirT1 is also capable of inducing browning of WAT, similar to TZDs. We report that SirT1-dependent Pparγ deacetylation promotes browning of subcutaneous WAT by regulating ligand-dependent coactivator/corepressor exchange at the Pparγ transcriptional complex. We propose that SirT1-dependent Pparγ deacetylation regulates energy homeostasis, promoting energy expenditure over energy storage.

RESULTS

SirT1 deacetylates Pparγ in a ligand-dependent manner

We investigated whether Pparγ activation by TZD ligands affects its acetylation. Indeed, treatment with rosiglitazone dose-dependently decreased Pparγ acetylation (Figure 1A). Moreover, Pparγ agonists facilitated, while the antagonist GW9662 prevented the interaction between Pparγ and SirT1 (Figures 1A and 1B). Pparγ acetylation was augmented by acetyltransferase Cbp (Figure 1C) or HDAC inhibitors trichostatin A (TSA) and nicotinamide (Figure S1A). Conversely, SirT1 overexpression or chemical activation with resveratrol decreased Pparγ acetylation levels (Figures 1C and S1B). To determine whether Pparγ is a SirT1 substrate, we performed *in vitro* deacetylation assays with purified SirT1 and acetylated Pparγ. The data demonstrate that WT, but not catalytically inactive mutant (H363Y) SirT1 deacetylates Pparγ in a NAD^+-dependent manner. The SirT1 inhibitor nicotinamide reversed the effect of SirT1 (Figures 1D and 1E). These findings

reveal that SirT1 deacetylates Pparγ. Unlike other SirT1 substrates, Pparγ requires agonist binding to engage SirT1 *in vivo*.

Next we asked whether SirT1 interacts with Pparγ in physiological conditions. Accordingly, we detected SirT1 in Pparγ immunoprecipitates from epididymal and inguinal WAT (eWAT and iWAT) lysates (Figure 1F). Taking advantage of Flag-tagged SirT1 in *SirT1* Bacterial Artificial Chromosome Overexpressor transgenic mice (*SirBACO*) (Banks et al., 2008), we demonstrated that Pparγ could be detected by *in vivo* co-immunoprecipitation of Flag-SirT1 in iWAT (Figure 1G).

SirT1 mimics the effects of Pparγ ligands on white and brown genes

Since both TZDs and SirT1 decrease Pparγ acetylation, we hypothesized that SirT1 gain-of-function phenocopies aspects of Pparγ activation by TZDs. A known function of TZDs is to repress visceral WAT genes whose induction is generally associated with insulin resistance (Vernochet et al., 2009). Activation of SirT1 by resveratrol in 3T3-L1 white adipocytes had a similar effect (Figure 2A). Overexpression of SirT1 did not affect adipogenesis (Figures S2A–S2C), but selectively decreased representative white genes *Angiotensinogen* (*Agt*), *Resistin, Wdnm1L, Chemerin* and *Pank3.* The catalytically inactive SirT1 mutant, H363Y, was unable to repress most white genes (Figure 2B). The inhibitory effect of SirT1 on these white genes is consistent with its lipid mobilizing function in white adipocyte (Picard et al., 2004). Next we compared the effects of SirT1 with those of Pparγ agonists on brown genes in HIB-1B cells (Tontonoz et al., 1994). We chose these cells because their expression levels of Ucp1, SirT1 and its native inhibitor Deleted in breast cancer-1 (Dbc1) (Kim et al., 2008; Zhao et al., 2008) are more similar to subcutaneous WAT (iWAT) than those of 3T3-L1 white adipocytes (Figure S2D). Activating SirT1 with resveratrol (Lagouge et al., 2006) or Pparγ with troglitazone increased *Ucp1* while the SirT1 inhibitor nicotinamide mimicked the Pparγ antagonist GW9662 to repress it (Figure 2C). Overexpression of WT or H363Y mutant SirT1 did not inhibit cellular differentiation (Figure S2E), but WT SirT1 decreased Pparγ acetylation and increased BAT markers *Ucp1* and *Dio2,* while the H363Y mutant had the opposite effect (Figures 2D and 2E). These data indicate that SirT1 deacetylase activity is required to promote brown gene expression and repress white genes in a cell-autonomous manner that mimics liganded Pparγ.

SirT1 induces ‘browning’ of subcutaneous WAT

In vivo, we observed a positive correlation of SirT1 levels with brown gene expression in different mouse adipose tissues; conversely, we observed a negative correlation of the SirT1 inhibitor Dbc1 with brown genes (Figures 3A and S3A). Based on these findings, we probed the browning function of SirT1 *in vivo* by using three mouse models of altered SirT1 activity: *Sirt1* knockout mice (*Sirt1*$^{-/-}$) (McBurney et al., 2003); mice with increased SirT1 activity as a result of genetic deletion of *Dbc1* (*Dbc1*$^{-/-}$) (Escande et al., 2010) and mice overexpressing SirT1 (*SirBACO*) (Banks et al., 2008). In rare *Sirt1*$^{-/-}$ mice that survived to adulthood (McBurney et al., 2003), we saw normal levels of brown markers Ucp1 and C/ebpβ in BAT (Figure S3B), but lower levels in iWAT (Figure 3B), indicating that SirT1 is required to maximize the thermogenic capacity of subcutaneous WAT.

To validate our finding, we surveyed adipose tissues in *Dbc1*$^{-/-}$ mice after triggering thermogenesis by overnight cold exposure (4°C). We saw increased numbers of Ucp1-immunoreactive paucilocular iWAT adipocytes, which are usually unilocular (Figure 3C), together with increased expression of brown genes *Ucp1* and *C/ebpβ*, andsuppression of white genes, *Chemerin* and *Resistin* (Figures 3D and 3F), suggestive of a “browning” of subcutaneous white adipocytes. In contrast, knockout of *Dbc1* had no effect on *Ucp1* expression in BAT (Figures S3C and S3D). We observed a similar induction of *Ucp1* and *C/*

ebpβ in visceral eWAT of *Dbc1*$^{-/-}$ mice (Figure S3E) but, unlike in subcutaneous iWAT, we saw no paucilocular adipocytes (Figure 3C). Owing to the extremely low levels of *Ucp1* in eWAT (Figures 3A and S3A), it's unlikely that its induction in this tissue contributes significantly to overall thermogenesis, consistent with the observation that iWAT is the WAT depot most prone to browning (Kozak, 2010). If the browning effect associated with *Dbc1* knockout was mediated by increased SirT1 activity, it should be phenocopied by SirT1 gain-of-function in *SirBACO* mice. Indeed, cold-exposed *SirBACO* mice had an increased number of Ucp1-immunoreactive paucilocular adipocytes in iWAT, as did *Dbc1*$^{-/-}$ mice (Figure 3C). The expression of brown markers, including *Ucp1, Dio2* and *C/ebpβ* was increased in iWAT of *SirBACO* mice (Figures 3E and 3G). Similar to *Sirt1*$^{-/-}$ and *Dbc1*$^{-/-}$ mice, *SirBACO* mice had only marginally enhanced expression of *Ucp1* and *C/ebpβ* in BAT (Figures S3F and S3G). Interestingly, Cbp-deficient mice–which are known to be insulin-sensitive–show similar browning phenotypes (Yamauchi et al., 2002). These data indicate a browning function of SirT1 in iWAT, rather than BAT.

SirT1 gain-of-function and Pparγ ligands have overlapping insulin-sensitizing effects

We next investigated the metabolic correlates of our findings. Aging *Dbc1*$^{-/-}$ mice become glucose intolerant without body weight changes (Figures 4A and S4A). We exploited this feature to critically test the hypothesis that promoting BAT-like features in WAT benefits insulin sensitivity. We exposed insulin-resistant *Dbc1*$^{-/-}$ mice and controls to 12°C, a moderately low temperature. Unlike acute cold exposure to 4°C, this treatment didn't result in loss of body weight (Figure S4A). The 4-week treatment had no effect in controls, but restored glucose tolerance in *Dbc1*$^{-/-}$ mice (Figures 4A and 4B), with increased expression of brown genes in iWAT (data not shown). In *SirBACO* mice, chronic cold exposure resulted in lesser weight gain (Figure S4B), despite increased food intake (Figure S4C), suggesting increased energy expenditure. Similar to acute cold exposure, we observed changes in iWAT, but not in BAT and eWAT (Figures S4D and S4E), associated with the appearance of smaller, paucilocular or multilocular adipocytes with more intense Ucp1 immunoreactivity (Figure 4C). Gene expression studies demonstrated elevated levels of brown (*Ucp1, Cox7a1* and *Cidea*), angiogenic (*Vegf*) and lipolytic genes (*Atgl*) (Figure 4D)–all indicative of improved WAT function along with brown remodeling.

WAT "insulin-resistance" genes were concordantly decreased (Figure 4D) in iWAT from *SirBACO* mice on high-fat diet (HFD) (Figure 4E), similar to their downregulation by Pparγ agonist (Vernochet et al., 2009). As expected, Pparγ acetylation was decreased in *SirBACO* mice (Figure 4F), presumably mirroring TZD's *in vitro* effect. If TZDs and SirT1-dependent Pparγ deacetylation promoted browning through a shared molecular mechanism, we would expect that the *in vivo* effects of TZDs would be partly offset by SirT1 gain-of-function, to the extent that they are both mediated by browning of adipose tissue. This hypothesis can only be tested indirectly, as the systemic effects of SirT1 and TZDs on insulin sensitivity are not limited to browning of WAT, nor are they exclusively mediated by one another (i.e., there are SirT1-independent effects of TZDs and vice versa). Nonetheless, we investigated the ability of rosiglitazone to restore glucose tolerance in *SirBACO* and *Dbc1*$^{-/-}$ mice rendered insulin-resistant with high fat feeding. Indeed, administration of rosiglitazone improved glucose tolerance in high-fat-fed *WT* mice, but had only partial, statistically non-significant effects in either *SirBACO* (Figures 4G, 4H, and S4F) or *Dbc1*$^{-/-}$ mice (Figures 4I, 4J, and S4G). These findings provide additional evidence for our hypothesis.

SirT1 deacetylates Pparγ on Lys268 and Lys293

We sought to identify SirT1-dependent deacetylation sites in Pparγ. We used HPLC/MS/MS analysis on trypsin– and chymotrypsin–digested peptides to identify five acetylated

lysines at residues 98, 107, 218, 268 and 293, with ~87% coverage of Pparγ sequence (Figure S5A-B). Among them, two evolutionally conserved residues in the helix 2-helix 2' region, Lys268 and Lys293 (Figure S5C), were deacetylated following rosiglitazone treatment (Figures 5A and 5B), suggesting that they are SirT1 substrates. In the Pparγ tertiary structure (Figure S5D), Lys268 juts out from the groove containing Ser273 (Lin et al., 2009; Nolte et al., 1998), a cyclin-dependent kinase 5 (CDK5) phosphorylation site (Choi et al., 2010), while Lys293 lies as a potential gatekeeper with its side chain facing Ser273. The loop following Pparγ helix 2' is highly flexible, and responds with different conformational changes to Pparγ ligands with distinct transcriptional signatures (Waku et al., 2009). Ligand binding induces a conformational change that hinders access to the groove, burying Lys293 (Figures 5C and S5E). It bears to reason that this event may require debulking acetylated Lys293 through deacetylation. Unlike Lys293, Lys291 anchors on the opposite side of helix 2', and upon ligand binding its long side chain abuts on the outside of the groove (Figures S5D and S5E). Consistently, mass spectroscopy analysis of Pparγ peptides showed that it is not acetylated (data now shown).

Humans carrying the Pparγ mutation P467L (Pro495 of murine Pparγ2) are severely insulin-resistant and diabetic (Barroso et al., 1999). This amino acid change disrupts a conserved coactivator-binding motif LxxLL (murine Pparγ's amino acids 493-497) in helix 12 (Figure S5F). Interestingly, SirT1 interacts with another transcription factor, FoxO1, through the latter's cognate LxxLL motif (Nakae et al., 2006). Thus, we asked whether the P467L mutation interferes with Pparγ binding to and deacetylation by SirT1. Protein interaction modeling localized binding of SirT1 to ligand-bound Pparγ within the LxxLL motif (Figure S5G). Indeed, P467L Pparγ was hyperacetylated, and showed reduced binding to SirT1 that failed to be rescued by SirT1 overexpression (Figure 5D). Alanine mutations of the LxxLL motif (L496A/L497A) also abolished the interaction of Pparγ and SirT1 (Figure 5E). Mutating Lys293 or Lys268 in the hyperacetylated Pparγ mutant P467L dramatically decreased its acetylation, providing further evidence that both residues are sites of Pparγ acetylation (Figure 5F). Of interest, Pro495 (Pro467 in human) and Lys293 are juxtaposed by a bridge between Ile295 and His494 and the aromatic side chain of Phe315 in response to ligand binding (Waku et al., 2009). This conformation should facilitate SirT1 binding to the LxxLL motif, providing ready access to its substrates, Lys293 and the nearby Lys268.

Physiological regulation of Pparγ acetylation

To evaluate the significance of Pparγ acetylation, we investigated its regulation by physiological cues. Pparγ acetylation decreased in iWAT when brown genes were activated by cold exposure (Figure 5G), while it increased with insulin resistance brought about by HFD (Figure 5G). The increase of Pparγ acetylation following HFD was associated with reduced interaction with SirT1 (Figure 5H) and was reversed by rosiglitazone administration (Figure 5I), *Dbc1* knockout (Figure 5J) or SirT1 overexpression (Figure 4F). Moreover, activation of SirT1 by resveratrol decreased Pparγ acetylation in human subcutaneous adipose tissue (Figure 5K), in agreement with the insulin-sensitizing effects of resveratrol in humans (Timmers et al., 2011). Total Pparγ acetylation changed relatively little *in vivo*, consistent with the mass spectrometry demonstration that only two of five lysine residues are responsive to rosiglitazone (Figure S5B).

BAT-like functions of Pparγ acetylation site mutants

We investigated the effects of Pparγ deacetylation in adipocytes by generating stable clones of Swiss-3T3 fibroblasts expressing WT Pparγ, or acetylation-mimetic K293Q (KQ), deacetylation-mimetic K293R (KR) and K268R/K293R (2KR) Pparγ mutants. WT Pparγ induced differentiation of Swiss 3T3 fibroblasts into adipocytes, as did KR, whereas KQ delayed it (Figures 6A and S6A). Strikingly, the 2KR mutant was more potent than WT

Pparγ in promoting lipid accumulation, increasing expression of the insulin-sensitizing adipokine, adiponectin, and promoting degradation of anti-adipogenic β-catenin (Liu et al., 2006) (Figures 6A and S6A). These data indicate that deacetylation is required for full Pparγ activation. Mitochondrial activity, as assessed by membrane potential, was inhibited by KQ, but enhanced by 2KR (Figure 6C). These findings were unrelated to mitochondrial biogenesis, assessed by measuring mitochondrial mass (Figure 6C), mitochondrial DNA, or mitochondrial protein content (Figures S6C and S6D). 2KR was more potent than WT to activate BAT genes including *Ucp1, Elovl3, Cidea, Cox7a1* and *Pgc1*α (Figures 6D and S6E). In contrast, KQ selectively repressed expression of BAT genes and induced expression of white genes without affecting canonical Pparγ targets (Figures 6D, 6E, and S6E-F). Consistent with the induction of BAT genes, basal mitochondrial respiration and maximal mitochondrial respiratory capacity increased in cells expressing 2KR, as did oligomycin-dependent (i.e., ATP synthesis inhibition-dependent) proton leak (Figure 6B). Another TZD-responsive gene, *Fgf21* (Wang et al., 2008) was likewise repressed by KQ and activated by 2KR (Figure 6D). In summary, these data indicate that SirT1-dependent deacetylation of Pparγ Lys268 and Lys293 mediates TZD–induced browning of white adipocytes, enhancing expression of characteristic BAT genes and repressing white "insulin resistance" genes.

SirT1-dependent deacetylation modulates Pparγ coactivator/corepressor exchange

Ser273 phosphorylation regulates Pparγ activity (Choi et al., 2010). Interestingly, Ser273 phosphorylation parallels acetylation of Lys293, but not of Lys268 (Figures S7A and S7B). Thus, we investigated whether the transcriptional selectivity and metabolic functions of Pparγ deacetylation are mediated through ligand-dependent Ser273 dephosphorylation. Dephosphorylation of Ser273 by TZD is required to induce adiponectin (Choi et al., 2010). In Swiss 3T3 cells, stable overexpression of Pparγ S273A (SA) or S273A/2KR (AR) mutants resulted in overlapping effects on adiponectin (Figure S7C). In contrast, the AR mutant trumped the effect of the SA mutant by activating brown genes (Figure S7D). These data indicate that Pparγ acetylation and Ser273 phosphorylation are coordinately promote adipokine production, while deacetylation is the main signal affecting brown gene expression.

Ligand binding induces Pparγ/Rxr dimerization and cofactor exchange. We hypothesized that Pparγ deacetylation might dial in specificity of brown gene expression through coactivator/corepressor recruitment. Prdm16 is a determinant of the brown adipocyte lineage (Seale et al., 2008) that has been shown to induce browning of subcutaneous WAT (Seale et al., 2011). We observed that Prdm16 binding to Pparγ was dependent on rosiglitazone (Figure 7A, lanes 1-2). Pparγ acetylation by Cbp prevented Prdm16 binding, but rosiglitazone was able to partly relieve the inhibition to an extent that was commensurate with Pparγ deacetylation (Figure 7A, lanes 3-4). Accordingly acetylation-defective Pparγ 2KR showed constitutive, ligand-independent binding to Prdm16 (Figure 7B). Likewise, Cbp blocked the Pparγ/Prdm16 interaction while SirT1 overexpression was able to rescue it (Figure 7C), supporting a key role of deacetylation in this process. SirT1 gain-of-function mimicked the effect of Pparγ ligand to promote Prdm16 binding while the Pparγ antagonist GW9662 blocked the effect of SirT1 (Figure 7D). In addition, we demonstrated that Pparγ could be detected in chromatin immunoprecipitates from the *Ucp1* enhancer (Chen et al., 2009) together with Prdm16 in HIB-1B cells expressing SirT1, but not its HY mutant (Figure 7E). In contrast, neither *in vivo* nor *in vitro* did we detect any interaction between Prdm16 and SirT1 (data not shown).

Site-directed mutagenesis of individual lysine residues demonstrated that Lys293, but not Lys268, was critical to recruit Prdm16 to Pparγ (Figure 7F). Transcriptional corepressor NCoR is an important component of the Pparγ complex. Thus, we investigated whether

acetylation of these two lysines affected NCoR binding. Intriguingly, mutating either lysine to arginine abolished the interaction of NCoR with Pparγ, suggesting that acetylation of both residues is required for this interaction (Figure 7E). Consistent with these data, Cbp increased NCoR binding to Pparγ, while SirT1 prevented it (Figure 7G). Therefore, deacetylation of Pparγ on Lys293 is required to recruit coactivator Prdm16, while deacetylation on Lys268 and Lys293 is required to clear corepressor NCoR. These data indicate that the acetylation state of Lys268 and Lys293 is critical for corepressor/coactivator exchange.

DISCUSSION

This study illustrates that SirT1 gain-of-function induces BAT-like remodeling of white adipocytes *in vivo* and *in vitro* by deacetylating Pparγ on Lys293 and Lys268. We identify SirT1 as a Pparγ deacetylase, whose effects mimic biochemical, cell biological, and physiological outcomes of ligand-dependent Pparγ activation. Mechanistically, this process is associated with recruitment of the brown cofactor Prdm16 and clearance of the corepressor NCoR from the Pparγ complex. We propose a model in which the metabolic benefits of SirT1, the browning function of Pparγ ligands and their ability to selectively recruit coactivator Prdm16 are subsumed under the unifying mechanism of Pparγ deacetylation (Figure 7H). SirT1 is activated by energy deficiency (Cohen et al., 2004) and deacetylates Pparγ at Lys268 and Lys293. Thus, we suggest that Pparγ acetylation on Lys268 and Lys293 is a signal of plenty, as it favors lipid storage and cell proliferation (Figure S6B). Conversely, deacetylation of Pparγ tilts the balance from energy storage to energy expenditure (thermogenesis) and promotes insulin sensitivity.

Pparγ deacetylation in browning WAT

Promoting brown features in white adipocytes can prevent obesity and diabetes (Farmer, 2009). In the present study, we propose a mechanism by which SirT1-mediated Pparγ deacetylation might contribute to this process. The browning function of SirT1 in WAT should be distinguished from its role in BAT since we didn't detect any effect of SirT1 gain- or loss-of-function in BAT in our mouse models. From a therapeutic standpoint, this is consistent with the idea that BAT itself plays a modest role in protecting from diet-induced weight gain, whereas converting WAT into a less efficient energy storage site might. It also suggests that browning of WAT occurs in a mechanistically distinct fashion from BAT activation. Indeed, several factors that promote WAT browning, such as Irisin (Bostrom et al., 2012), Fgf21 (Fisher et al., 2012) and Prdm16 (Seale et al., 2011) do so independently of BAT.

Unlike the browning factors mentioned above, SirT1 does not constitutively induce brown genes in iWAT at ambient temperature (not shown), suggesting that hormonal or environmental cues–such as cold exposure–are required to activate SirT1-dependent mechanisms of iWAT browning. Pparγ acetylation on Lys268 and Lys293 could therefore be exploited as readout to identify factors that modulate the browning process. The ability to regulate browning of WAT should be viewed as an essential component of any therapeutic approach that leverages this mechanism, since “browned” cells are energy inefficient, and might have undesired effects if left unchecked.

The SirT1-dependent browning process occurs in a heterogeneous fashion within morphologically and anatomically homogeneous adipose depots. This might be related to sympathetic innervation, a key modulator of BAT and Ucp1 induction in WAT (Bartness et al., 2010). Or it is possible that the ability to activate the brown program in response to Pparγ ligand or SirT1 gain-of-function is limited to a specialized subset of adipocytes. Alternatively, since vascular endothelial cells have pluripotent potential and can differentiate

into pre-adipocytes (Tran et al., 2012), activation of SirT1 and Pparγ deacetylation could favor pre-adipocyte differentiation into brown (or “brite”) adipocytes. This possibility is unlikely to account for brown gene induction in WAT following acute cold exposure, but might underlie the chronic effect of cold exposure.

Integrating acetylation with other post-translational modalities of Pparγ regulation

Lysine residues can be modified by sumoylation and ubiquitination. Fgf21 (Dutchak et al., 2012) and TZDs (Pascual et al., 2005) are insulin-sensitizers with browning properties (Fisher et al., 2012; Vernochet et al., 2009) that promote Pparγ sumoylation. The Fgf21-dependent sumoylation site on Pparγ, Lys107 (Dutchak et al., 2012), is strongly acetylated in our mass spectrometry analysis, but its acetylation is unaffected by rosiglitazone. It will be of interest to determine whether there exists a reciprocal regulation of acetylation and sumoylation at this site during the browning process. Ligand activation of Pparγ increases its ubiquitin-mediated degradation (Hauser et al., 2000), a process that could also be regulated by deacetylation of Lys268 and Lys293, as we observed that mutation of these two residues increased Pparγ stability (data not shown).

TZDs inhibit CDK5-dependent phosphorylation of Pparγ Ser273 (Choi et al., 2010), a residue buried within the groove lined by Lys268 and Lys293. Consistent with prior results in different systems (Qiang et al., 2010; Qiang et al., 2011), we show that Ser273 phosphorylation correlates with Lys293 acetylation, suggesting that the acetylation state of these two residues might affect access of related kinases or phosphatases, to the phosphorylation site. We also found that the effects of acetylation and phosphorylation of these residues on brown gene expression diverge, while those on the regulation of adiponectin overlap. Therefore, acetylation of Pparγ regulates its phosphorylation-mediated function. In summary, acetylation might integrate energy status with ligand availability to regulate protein stability and the effects of sumoylation and phosphorylation on Pparγ activity.

Therapeutic implications

Following the introduction of biguanides in the clinical management of diabetes in the 1940's, TZDs represent the only addition to the pharmacopeia of insulin-sensitizers. But their use has been tainted by liver toxicity, adverse effects on fluid balance, body weight, bone turnover and certain types of cancer, as well as lingering if elusive links to cardiovascular risk (Rosen, 2010). In addition, the TZD saga has negatively impacted development of transcription factor–based therapeutics, even as recognition of their homeostatic role has grown exponentially (Kim-Muller and Accili, 2011). Our data don't amount to a rehabilitation of TZDs for treatment of metabolic disorders, but raise the interesting possibility that, by judicious use of SirT1 agonists in combination with appropriate Pparγ ligands, it is possible to render WAT less efficient, thus warding off TZDs’ adverse effects and paving the way for a reevaluation of Pparγ as a therapeutic target (Qiang and Accili, 2012).

EXPERIMENTAL PROCEDURES

Experimental Animals

SirBACO mice (C57BL/6J background), *Dbc1*$^{-/-}$and *Sirt1*$^{-/-}$ mice (129/J × C57BL/6J background) were housed at 23±1°C in a 12-hr light/dark cycle with free access to normal chow (PicoLab rodent diet 20) (LabDiet 5053). The Columbia University Animal Care and Utilization Committee approved all procedures. High fat diet contained 60% calories from fat, 20% from protein and 20% carbohydrates (Research Diet, D12492). For acute cold exposure, we placed animals at 4°C for 16 hr, and for chronic cold exposure we placed

animals at 12°C on a 12-hr light/diet cycle for four weeks. We injected rosiglitazone intraperitoneally (i.p.) daily at a dose of 10 mg/kg body weight, performed IPGTT as described (Banks et al., 2008), and determined body compositions by NMR (Bruker Optics).

Plasmids and Cell Culture

We obtained pcDNA-Flag-Pparγ2 (# 8895), pBabe-puro-Flag-HA-Pparγ2 (# 8859) and pcDNA-Prdm16 (#15503) from Addgene, and generated Pparγ mutants K293R, K293Q, K268R, K268Q, 2KR (K268R/K293R), P467L, P467L/K293R and P467L/K268Q, S273A, S273A/K268R/K293R (AR) and L496A/L497A (2LA) by site-directed mutagenesis. In this study, Pparγ refers to the longer isoform Pparγ2. We subcloned WT and H363Y mutant SirT1 cDNA into the *BamH*I site of pEGFP-N1 to generate N-terminal FLAG- and C-terminal GFP-tagged SirT1. We cloned these constructs into plasmid pBabe-blast, modified by replacing the puromycin-resistance gene with a blasticidin-resistance gene, to engineer retroviral vectors for derivation of stably transduced clones as described (Vernochet et al., 2009). The final concentration of puromycin or blasticidin for selection is 2.5 μg/mL. HA-Pparγ (Kitamura et al., 2005) and SirT1 adenoviruses have been described (Nakae et al., 2003). For transient expression in HEK-293T (293) cells, we transfected pcDNA-Pparγ or pEGFP-SirT1 using *Trans*IT-LT1 reagent (Mirus Bio), or transduced Pparγ or SirT1 adenoviruses. We differentiated and maintained 3T3-L1 preadipocytes, Swiss-3T3 fibroblasts (both from ATCC), and HIB-1B brown preadipocytes as described (Vernochet et al., 2009). We treated cells overnight with resveratrol (10 μM), troglitazone (10 μM), rosiglitazone (5 μM), nicotinamide (20 mM), or GW9662 (10 μM).

Protein Analysis

We extracted proteins and performed western blotting as described (Qiang et al., 2010). Sources of antibodies are: Dbc1 (Bethyl Laboratories); Ucp1 (Abcam); Adiponectin (Affinity BioReagents); SirT1 and β-catenin (Millipore); Flag M2 and HA (Sigma-Aldrich); Prdm16 (R&D systems); monoclonal or polyclonal Acetyl-lysine, aP2, Perilipin and phospho-CDK substrate (Cell Signaling); actin, tubulin, C/ebpβ, Pparγ (E8), Pparγ (H100), NCoR and Cox III (Santa Cruz).

Immunoprecipitation and *in vivo* Pparγ Acetylation

We performed Co-immunoprecipitation (Co-IP) in Flag IP buffer (50 mM Tris pH7.9, 150 mM NaCl, 10% glycerol supplemented with protease inhibitors). For immunoprecipitation (IP), we lysed cells into high-salt Flag IP buffer. To detect Pparγ acetylation *in vivo*, we extracted proteins from adipose tissues into high-salt Flag IP buffer and delipidated them by ultracentrifugation (40,000 rpm for 2 hours at 4°C). We incubated lysates with antibody-conjugated agarose beads overnight at 4°C, washed the beads four times and eluted the precipitates by Flag/HA peptides or boiling in non-reducing sample buffer. The antibody-conjugated agarose beads are: Flag M2 beads and monoclonal Anti-HA (Sigma-Aldrich), Pparγ (H100)-conjugated (Santa Cruz) and anti-acetyl Lysine agarose (ImmuneChem).

Gene Expression Analysis

We isolated RNA with RNeasy Lipid Tissue kit (Qiagen) and DNase I digestion, synthesized cDNA with High-capacity cDNA Reverse Transcription kit (Applied Biosystems), and performed quantitative real-time PCR (Q-PCR) with goTaq qPCR Master Mix (Promega) in a Bio-Rad CFX96 Real-Time PCR system. We calculated relative gene expression levels by ΔΔCt method using cyclophilin A as internal control. We list primer sequences in Table S1.

Histology

We used paraffin-embedded sections for H&E, and Ucp1 immunohistochemistry (Abcam, 1:100 dilution). We assessed adipocyte lipid content by Oil red-O staining.

Statistical analysis

We used unpaired 2-tail student's *t*-tests to evaluate statistical significance and $P<0.05$ to declare a statistically significant change. We present all values as means ± standard error of means (SEM).

Supplementary Material

Refer to Web version on PubMed Central for supplementary material.

Acknowledgments

We thank K. Tsuchiya and L. Ozcan for help with different aspects of this work, T. Kolar and A. Flete for technical support, Q. Zhang for help with structural analysis, U. Pajvani and G. Heinrich for comments on the manuscript and members of the Accili laboratory for discussion of the data. We thank B. Spiegelman for providing HIB-1B cells. This work was supported by NIH grants HL087123, DK58282, DK64773, DK063608 (Columbia Diabetes Research Center), and RR024156 (Columbia University CTSA).

REFERENCES

Banks AS, Kon N, Knight C, Matsumoto M, Gutierrez-Juarez R, Rossetti L, Gu W, Accili D. SirT1 gain of function increases energy efficiency and prevents diabetes in mice. Cell Metab. 2008; 8:333–341. [PubMed: 18840364]

Barroso I, Gurnell M, Crowley VE, Agostini M, Schwabe JW, Soos MA, Maslen GL, Williams TD, Lewis H, Schafer AJ, et al. Dominant negative mutations in human PPARgamma associated with severe insulin resistance, diabetes mellitus and hypertension. Nature. 1999; 402:880–883. [PubMed: 10622252]

Bartness TJ, Vaughan CH, Song CK. Sympathetic and sensory innervation of brown adipose tissue. Int J Obes (Lond). 2010; 34(Suppl 1):S36–42. [PubMed: 20935665]

Bostrom P, Wu J, Jedrychowski MP, Korde A, Ye L, Lo JC, Rasbach KA, Bostrom EA, Choi JH, Long JZ, et al. A PGC1-alpha-dependent myokine that drives brown-fat-like development of white fat and thermogenesis. Nature. 2012; 481:463–468. [PubMed: 22237023]

Canto C, Gerhart-Hines Z, Feige JN, Lagouge M, Noriega L, Milne JC, Elliott PJ, Puigserver P, Auwerx J. AMPK regulates energy expenditure by modulating NAD+ metabolism and SIRT1 activity. Nature. 2009; 458:1056–1060. [PubMed: 19262508]

Cederberg A, Gronning LM, Ahren B, Tasken K, Carlsson P, Enerback S. FOXC2 is a winged helix gene that counteracts obesity, hypertriglyceridemia, and diet-induced insulin resistance. Cell. 2001; 106:563–573. [PubMed: 11551504]

Chen W, Yang Q, Roeder RG. Dynamic interactions and cooperative functions of PGC-1alpha and MED1 in TRalpha-mediated activation of the brown-fat-specific UCP-1 gene. Molecular cell. 2009; 35:755–768. [PubMed: 19782026]

Choi JH, Banks AS, Estall JL, Kajimura S, Bostrom P, Laznik D, Ruas JL, Chalmers MJ, Kamenecka TM, Bluher M, et al. Anti-diabetic drugs inhibit obesity-linked phosphorylation of PPARgamma by Cdk5. Nature. 2010; 466:451–456. [PubMed: 20651683]

Cohen HY, Miller C, Bitterman KJ, Wall NR, Hekking B, Kessler B, Howitz KT, Gorospe M, de Cabo R, Sinclair DA. Calorie restriction promotes mammalian cell survival by inducing the SIRT1 deacetylase. Science. 2004; 305:390–392. [PubMed: 15205477]

Dutchak PA, TKatafuchi T, Bookout AL, Choi JH, Yu RT, Mangelsdorf D, Kliewer SA. Fibroblast Growth Factor-21 Regulates PPARγ Activity and the Antidiabetic Actions of Thiazolidinediones. Cell. 2012; 148:556–567. [PubMed: 22304921]

Escande C, Chini CC, Nin V, Dykhouse KM, Novak CM, Levine J, van Deursen J, Gores GJ, Chen J, Lou Z, et al. Deleted in breast cancer-1 regulates SIRT1 activity and contributes to high-fat diet-induced liver steatosis in mice. The Journal of clinical investigation. 2010; 120:545–558. [PubMed: 20071779]

Farmer SR. Obesity: Be cool, lose weight. Nature. 2009; 458:839–840. [PubMed: 19370020]

Fisher FM, Kleiner S, Douris N, Fox EC, Mepani RJ, Verdeguer F, Wu J, Kharitonenkov A, Flier JS, Maratos-Flier E, et al. FGF21 regulates PGC-1alpha and browning of white adipose tissues in adaptive thermogenesis. Genes Dev. 2012; 26:271–281. [PubMed: 22302939]

Hauser S, Adelmant G, Sarraf P, Wright HM, Mueller E, Spiegelman BM. Degradation of the peroxisome proliferator-activated receptor gamma is linked to ligand-dependent activation. J Biol Chem. 2000; 275:18527–18533. [PubMed: 10748014]

Kim JE, Chen J, Lou Z. DBC1 is a negative regulator of SIRT1. Nature. 2008; 451:583–586. [PubMed: 18235501]

Kim-Muller JY, Accili D. Cell biology. Selective insulin sensitizers. Science. 2011; 331:1529–1531. [PubMed: 21436429]

Kitamura YI, Kitamura T, Kruse JP, Raum JC, Stein R, Gu W, Accili D. FoxO1 protects against pancreatic beta cell failure through NeuroD and MafA induction. Cell Metab. 2005; 2:153–163. [PubMed: 16154098]

Kozak LP. Brown fat and the myth of diet-induced thermogenesis. Cell metabolism. 2010; 11:263–267. [PubMed: 20374958]

Lagouge M, Argmann C, Gerhart-Hines Z, Meziane H, Lerin C, Daussin F, Messadeq N, Milne J, Lambert P, Elliott P, et al. Resveratrol improves mitochondrial function and protects against metabolic disease by activating SIRT1 and PGC-1alpha. Cell. 2006; 127:1109–1122. [PubMed: 17112576]

Lin YY, Lu JY, Zhang J, Walter W, Dang W, Wan J, Tao SC, Qian J, Zhao Y, Boeke JD, et al. Protein acetylation microarray reveals that NuA4 controls key metabolic target regulating gluconeogenesis. Cell. 2009; 136:1073–1084. [PubMed: 19303850]

Liu J, Wang H, Zuo Y, Farmer SR. Functional interaction between peroxisome proliferator-activated receptor gamma and beta-catenin. Molecular and cellular biology. 2006; 26:5827–5837. [PubMed: 16847334]

McBurney MW, Yang X, Jardine K, Hixon M, Boekelheide K, Webb JR, Lansdorp PM, Lemieux M. The mammalian SIR2alpha protein has a role in embryogenesis and gametogenesis. Molecular and cellular biology. 2003; 23:38–54. [PubMed: 12482959]

Milne JC, Lambert PD, Schenk S, Carney DP, Smith JJ, Gagne DJ, Jin L, Boss O, Perni RB, Vu CB, et al. Small molecule activators of SIRT1 as therapeutics for the treatment of type 2 diabetes. Nature. 2007; 450:712–716. [PubMed: 18046409]

Nakae J, Cao Y, Daitoku H, Fukamizu A, Ogawa W, Yano Y, Hayashi Y. The LXXLL motif of murine forkhead transcription factor FoxO1 mediates Sirt1-dependent transcriptional activity. The Journal of clinical investigation. 2006; 116:2473–2483. [PubMed: 16917544]

Nakae J, Kitamura T, Kitamura Y, Biggs WH 3rd, Arden KC, Accili D. The forkhead transcription factor Foxo1 regulates adipocyte differentiation. Dev Cell. 2003; 4:119–129. [PubMed: 12530968]

Nolte RT, Wisely GB, Westin S, Cobb JE, Lambert MH, Kurokawa R, Rosenfeld MG, Willson TM, Glass CK, Milburn MV. Ligand binding and co-activator assembly of the peroxisome proliferator-activated receptor-gamma. Nature. 1998; 395:137–143. [PubMed: 9744270]

Pascual G, Fong AL, Ogawa S, Gamliel A, Li AC, Perissi V, Rose DW, Willson TM, Rosenfeld MG, Glass CK. A SUMOylation-dependent pathway mediates transrepression of inflammatory response genes by PPAR-gamma. Nature. 2005; 437:759–763. [PubMed: 16127449]

Picard F, Gehin M, Annicotte J, Rocchi S, Champy MF, O'Malley BW, Chambon P, Auwerx J. SRC-1 and TIF2 control energy balance between white and brown adipose tissues. Cell. 2002; 111:931–941. [PubMed: 12507421]

Picard F, Kurtev M, Chung N, Topark-Ngarm A, Senawong T, Machado De Oliveira R, Leid M, McBurney MW, Guarente L. Sirt1 promotes fat mobilization in white adipocytes by repressing PPAR-gamma. Nature. 2004; 429:771–776. [PubMed: 15175761]

Powelka AM, Seth A, Virbasius JV, Kiskinis E, Nicoloro SM, Guilherme A, Tang X, Straubhaar J, Cherniack AD, Parker MG, et al. Suppression of oxidative metabolism and mitochondrial biogenesis by the transcriptional corepressor RIP140 in mouse adipocytes. The Journal of clinical investigation. 2006; 116:125–136. [PubMed: 16374519]

Qiang L, Accili D. FGF21 and the Second Coming of PPARgamma. Cell. 2012; 148:397–398. [PubMed: 22304910]

Qiang L, Banks AS, Accili D. Uncoupling of acetylation from phosphorylation regulates FoxO1 function independent of its subcellular localization. The Journal of biological chemistry. 2010; 285:27396–27401. [PubMed: 20519497]

Qiang L, Lin HV, Kim-Muller JY, Welch CL, Gu W, Accili D. Proatherogenic abnormalities of lipid metabolism in SirT1 transgenic mice are mediated through Creb deacetylation. Cell metabolism. 2011; 14:758–767. [PubMed: 22078933]

Ravussin E, Galgani JE. The implication of brown adipose tissue for humans. Annual review of nutrition. 2011; 31:33–47.

Rosen CJ. Revisiting the rosiglitazone story--lessons learned. The New England journal of medicine. 2010; 363:803–806. [PubMed: 20660395]

Scime A, Grenier G, Huh MS, Gillespie MA, Bevilacqua L, Harper ME, Rudnicki MA. Rb and p107 regulate preadipocyte differentiation into white versus brown fat through repression of PGC-1alpha. Cell metabolism. 2005; 2:283–295. [PubMed: 16271529]

Seale P, Bjork B, Yang W, Kajimura S, Chin S, Kuang S, Scime A, Devarakonda S, Conroe HM, Erdjument-Bromage H, et al. PRDM16 controls a brown fat/skeletal muscle switch. Nature. 2008; 454:961–967. [PubMed: 18719582]

Seale P, Conroe HM, Estall J, Kajimura S, Frontini A, Ishibashi J, Cohen P, Cinti S, Spiegelman BM. Prdm16 determines the thermogenic program of subcutaneous white adipose tissue in mice. J Clin Invest. 2011; 121:96–105. [PubMed: 21123942]

Timmers S, Konings E, Bilet L, Houtkooper RH, van de Weijer T, Goossens GH, Hoeks J, van der Krieken S, Ryu D, Kersten S, et al. Calorie restriction-like effects of 30 days of resveratrol supplementation on energy metabolism and metabolic profile in obese humans. Cell Metab. 2011; 14:612–622. [PubMed: 22055504]

Tontonoz P, Graves RA, Budavari AI, Erdjument-Bromage H, Lui M, Hu E, Tempst P, Spiegelman BM. Adipocyte-specific transcription factor ARF6 is a heterodimeric complex of two nuclear hormone receptors, PPAR gamma and RXR alpha. Nucleic Acids Res. 1994; 22:5628–5634. [PubMed: 7838715]

Tran KV, Gealekman O, Frontini A, Zingaretti MC, Morroni M, Giordano A, Smorlesi A, Perugini J, De Matteis R, Sbarbati A, et al. The vascular endothelium of the adipose tissue gives rise to both white and brown fat cells. Cell Metab. 2012; 15:222–229. [PubMed: 22326223]

Tsukiyama-Kohara K, Poulin F, Kohara M, DeMaria CT, Cheng A, Wu Z, Gingras AC, Katsume A, Elchebly M, Spiegelman BM, et al. Adipose tissue reduction in mice lacking the translational inhibitor 4E-BP1. Nature medicine. 2001; 7:1128–1132.

Vernochet C, Peres SB, Davis KE, McDonald ME, Qiang L, Wang H, Scherer PE, Farmer SR. C/EBPalpha and the corepressors CtBP1 and CtBP2 regulate repression of select visceral white adipose genes during induction of the brown phenotype in white adipocytes by peroxisome proliferator-activated receptor gamma agonists. Mol Cell Biol. 2009; 29:4714–4728. [PubMed: 19564408]

Virtanen KA, Nuutila P. Brown adipose tissue in humans. Curr Opin Lipidol. 2011; 22:49–54. [PubMed: 21157334]

Waku T, Shiraki T, Oyama T, Fujimoto Y, Maebara K, Kamiya N, Jingami H, Morikawa K. Structural insight into PPARgamma activation through covalent modification with endogenous fatty acids. J Mol Biol. 2009; 385:188–199. [PubMed: 18977231]

Wang H, Qiang L, Farmer SR. Identification of a domain within peroxisome proliferator-activated receptor gamma regulating expression of a group of genes containing fibroblast growth factor 21 that are selectively repressed by SIRT1 in adipocytes. Molecular and cellular biology. 2008; 28:188–200. [PubMed: 17954559]

Wang YC, McPherson K, Marsh T, Gortmaker SL, Brown M. Health and economic burden of the projected obesity trends in the USA and the UK. Lancet. 2011; 378:815–825. [PubMed: 21872750]

Yamauchi T, Oike Y, Kamon J, Waki H, Komeda K, Tsuchida A, Date Y, Li MX, Miki H, Akanuma Y, et al. Increased insulin sensitivity despite lipodystrophy in Crebbp heterozygous mice. Nat Genet. 2002; 30:221–226. [PubMed: 11818964]

Zhao W, Kruse JP, Tang Y, Jung SY, Qin J, Gu W. Negative regulation of the deacetylase SIRT1 by DBC1. Nature. 2008; 451:587–590. [PubMed: 18235502]

Highlights

- SirT1 promotes browning of white fat
- SirT1 deacetylates liganded Pparγ
- SirT1 and Pparγ coordinately induce browning of white adipose
- Therapeutic potential of TZD and SirT1 agonist combination therapy for obesity

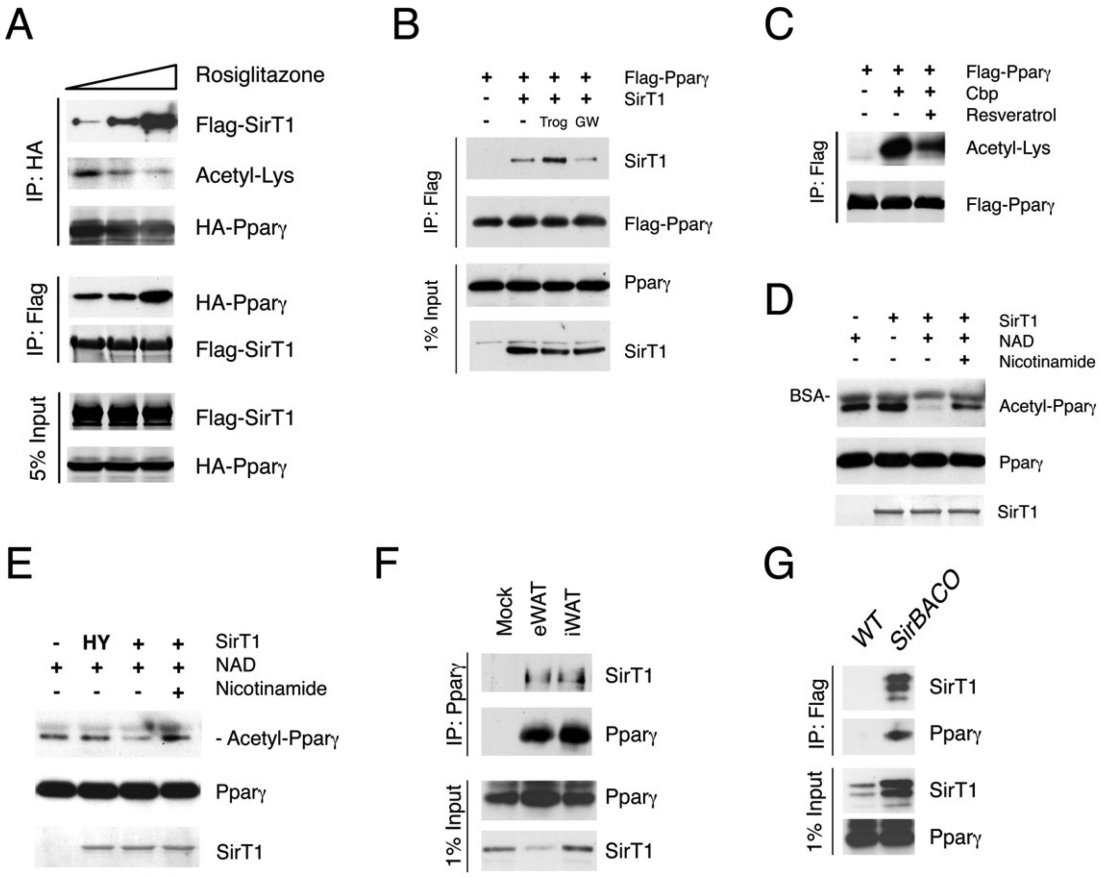

Figure 1. SirT1 deacetylates Pparγ in a ligand-dependent manner

(A) Co-immunoprecipitation (Co-IP) of Flag-tagged SirT1 or HA-tagged Pparγ in response to overnight rosiglitazone treatment in 293 cells.

(B) Co-IP of Flag-Pparγ and SirT1 in 293 cells treated with troglitazone (Trog) or GW9662 (GW) overnight.

(C) Pparγ acetylation in 293 cells in response to resveratrol.

(D-E) *In vitro* Pparγ deacetylation by SirT1. Bovine serum albumin (BSA) is contained in the reaction buffer.

(F) Co-IP of Pparγ with SirT1 in mouse adipose tissues. We immunoprecipitated 2 mg of epididymal (eWAT) or inguinal fat lysates (iWAT) with Pparγ antibody H100, and blotted the immunoprecipitates with SirT1 or Pparγ (E8) antibodies.

(G) Co-IP of SirT1 and Pparγ with Flag M2 beads using iWAT (5 mg) from *SirBACO* mice expressing Flag-tagged SirT1.

See also Figure S1.

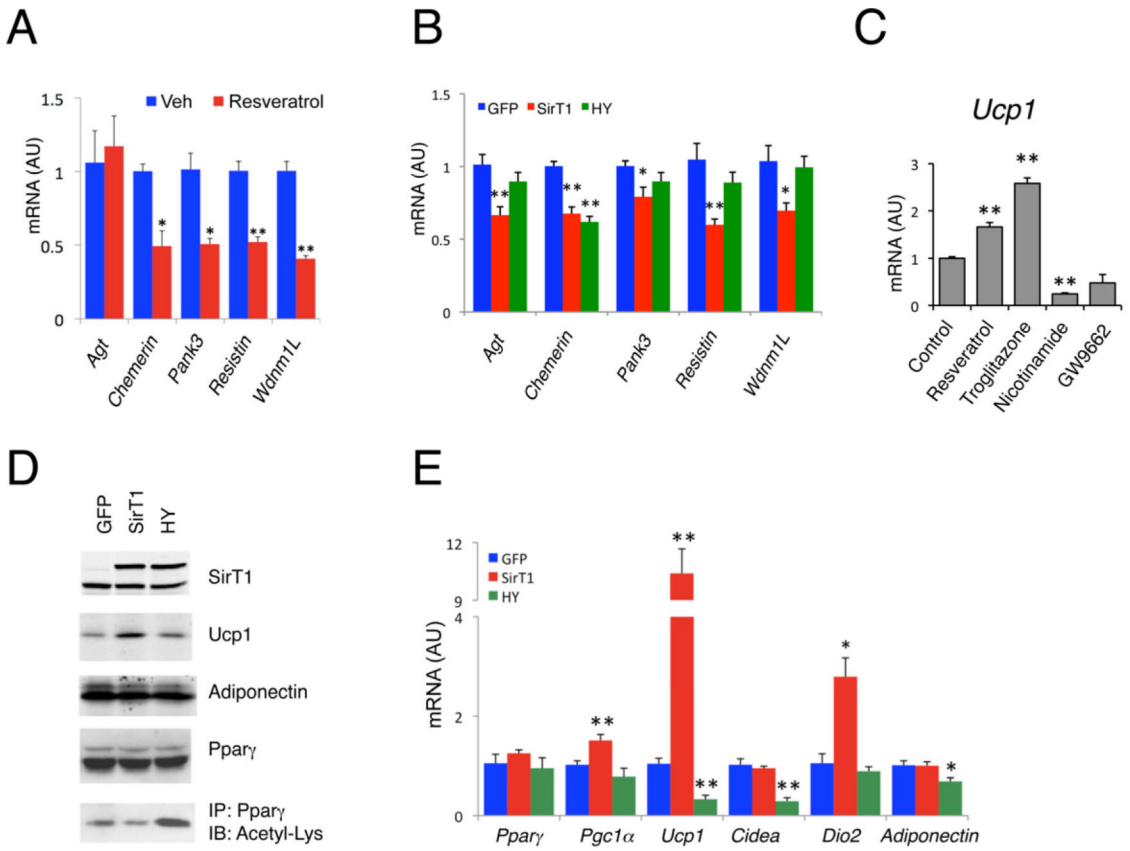

Figure 2. SirT1 mimics Pparγ ligand in regulating adipocyte gene expression

(A) Expression of white genes in 3T3-L1 adipocytes treated with 50 μM resveratrol or vehicle (Veh) overnight on differentiation day 7. *: $P<0.05$, **: $P<0.01$ *vs.* vehicle (n=3).

(B) White gene expression in 3T3-L1 adipocytes overexpressing GFP, SirT1 or Sirt1-H363Y (HY). Fully differentiated cells were harvested on day 8 of differentiation. *: $P<0.05$, **: $P<0.01$ *vs.* GFP (n=7).

(C) *Ucp1* expression in HIB-1B brown adipocytes with treatments overnight on day 6 of differentiation. **: $P<0.01$ *vs.* vehicle-treated controls (n=3-4).

(D-E) Protein (D) and gene expression analysis (E) in HIB-1B cells overexpressing GFP, SirT1 and Sirt1-H363Y (HY). IP: immunoprecipitation, IB: immunoblot; *: $P<0.05$, **: $P<0.01$ *vs.* GFP (n=3-9). Values are presented as means ± SEM.

See also Figure S2.

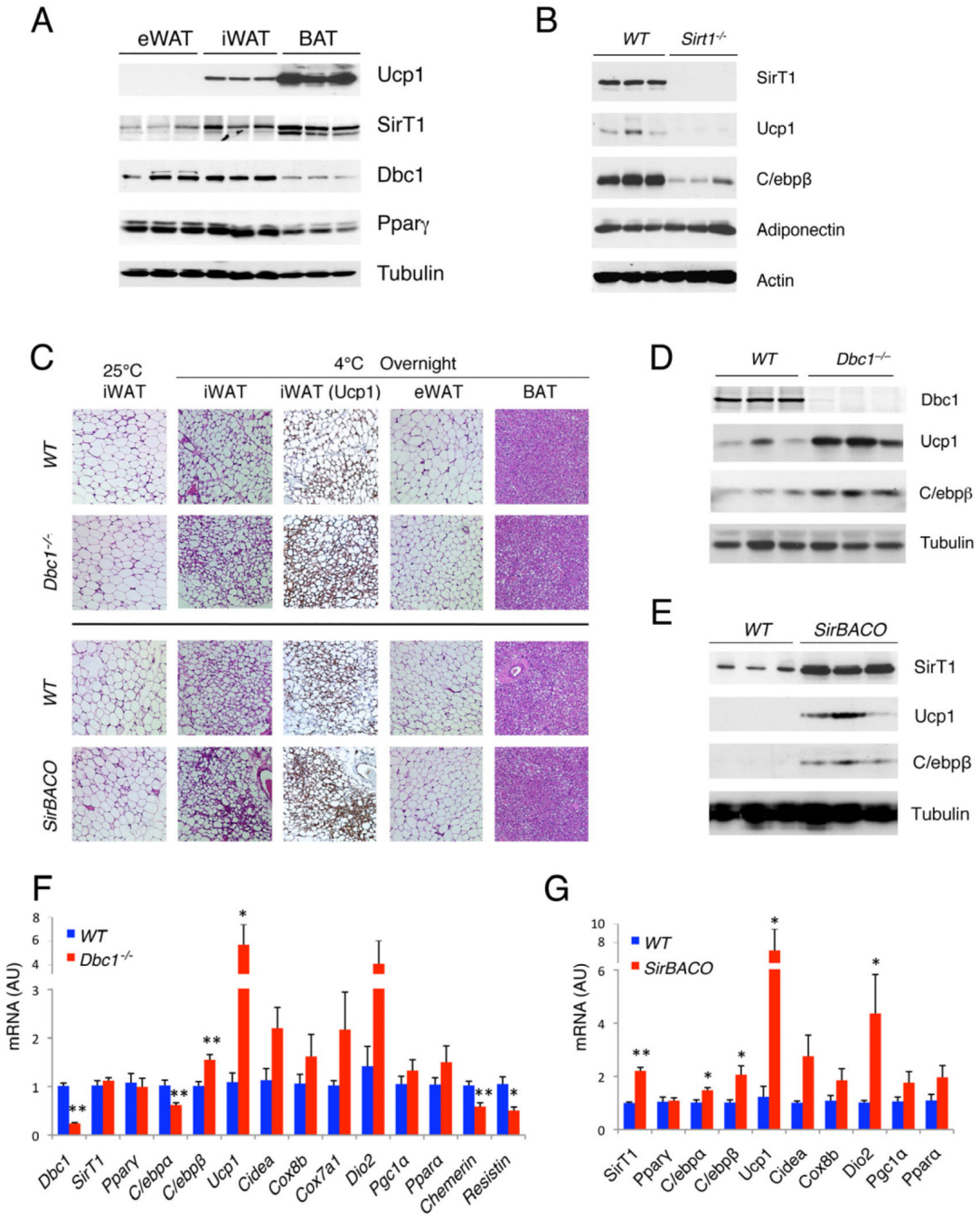

Figure 3. SirT1 gain-of-function promotes browning of subcutaneous WAT

(A) Western blots in visceral (eWAT), subcutaneous (iWAT) and brown (BAT) adipose tissues from cold-exposed 8-week-old male mice.

(B) Western blotting of iWAT from chow-fed *SirT1*$^{-/-}$ mice and control littermates after overnight cold exposure.

(C-G) 8-week-old, chow-fed male *Dbc1*$^{-/-}$ and *SirBACO* mice with their control littermates (*WT*) were exposed to 4°C overnight. Haemotoxylin Eosin (H&E) and Ucp1 immunohistochemical staining of adipose tissues (C), western blotting (D-E) and gene expression analysis (F-G) of iWAT. *: $P<0.05$, **: $P<0.01$ for *Dbc1*$^{-/-}$ vs. *WT* (n=6) or for *SirBACO* vs. *WT* (n=5). Values are presented as means ± SEM.

See also Figure S3.

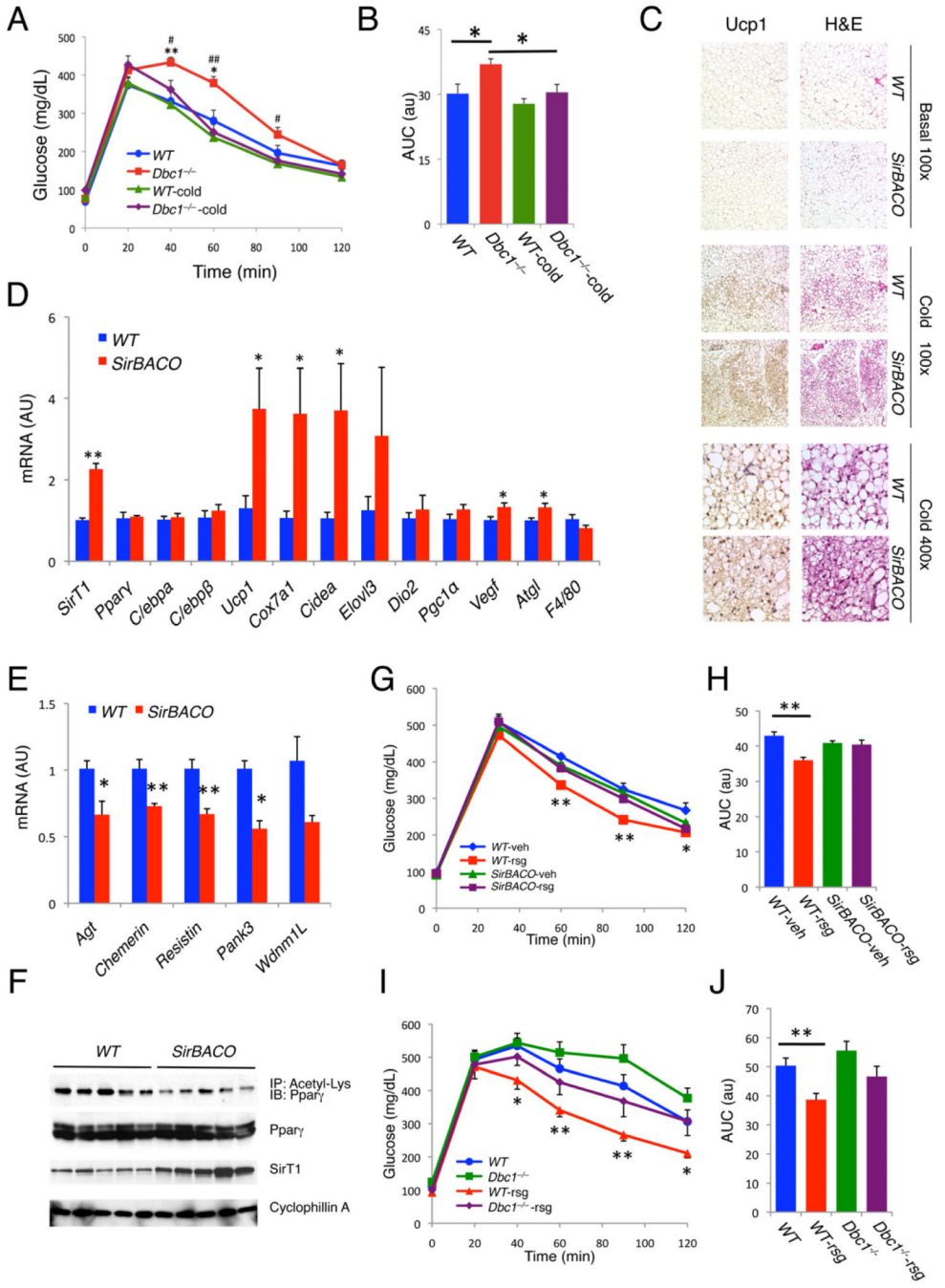

Figure 4. Metabolic correlates of SirT1-dependent Pparγ deacetylation

(A-B) Time course (A) and area under the curve (AUC) (B) of intra-peritoneal glucose tolerance tests (IPGTT) in chow-fed, 18-week-old male *Dbc1*$^{-/-}$ and WT mice before and after chronic cold exposure (12 °C for 4 weeks). Body weights are shown in Figure S4A. In Figure A *: P<0.05, **: P<0.01 for *Dbc1*$^{-/-}$ vs. *WT* before cold exposure; #: P<0.05, ##: P<0.01 for *Dbc1*$^{-/-}$ vs. cold-exposed *Dbc1*$^{-/-}$ mice. In Figure B, *: P<0.05. (n=6-7).

(C-D) Ucp1 immunohistochemistry, H&E staining (C), and gene expression (D) in iWAT of 9-week-old male *SirBACO* mice after chronic cold exposure. *: P<0.05, **: P<0.01 vs. *WT* (n=6).

(E-F) Expression of white genes (E) and Pparγ acetylation (F) in iWAT of male *SirBACO* mice after 8 weeks on high-fat diet (HFD). Mice were placed on HFD at 6 weeks of age. *: $P<0.05$, **: $P<0.01$ vs. *WT* (n=5). IP: Immunoprecipitation, IB: immunoblot.
(G-H) IPGTT (G) and AUC (H) in male *SirBACO* mice fed with HFD for 6 weeks (starting at 12 weeks of age), and treated with rosiglitazone (rsg) or vehicle (veh) for 1 week. Body weight information is in Figure S4F. *: $P<0.05$, **: $P<0.01$ *WT*-rsg *vs.* *WT*-veh (n=6-8).
(I-J) IPGTTs (I) and AUC (J) in male $Dbc1^{-/-}$ mice fed with HFD for 25 weeks before and after 1 week rosiglitazone (rsg) administration. Mice were placed on HFD at 5 weeks of age. Body weight information is in Figure S4G. *: $P<0.05$, **: $P<0.01$ for *WT vs.* *WT*-rsg (n=7).
Values are presented as means ± SEM.
See also Figure S4.

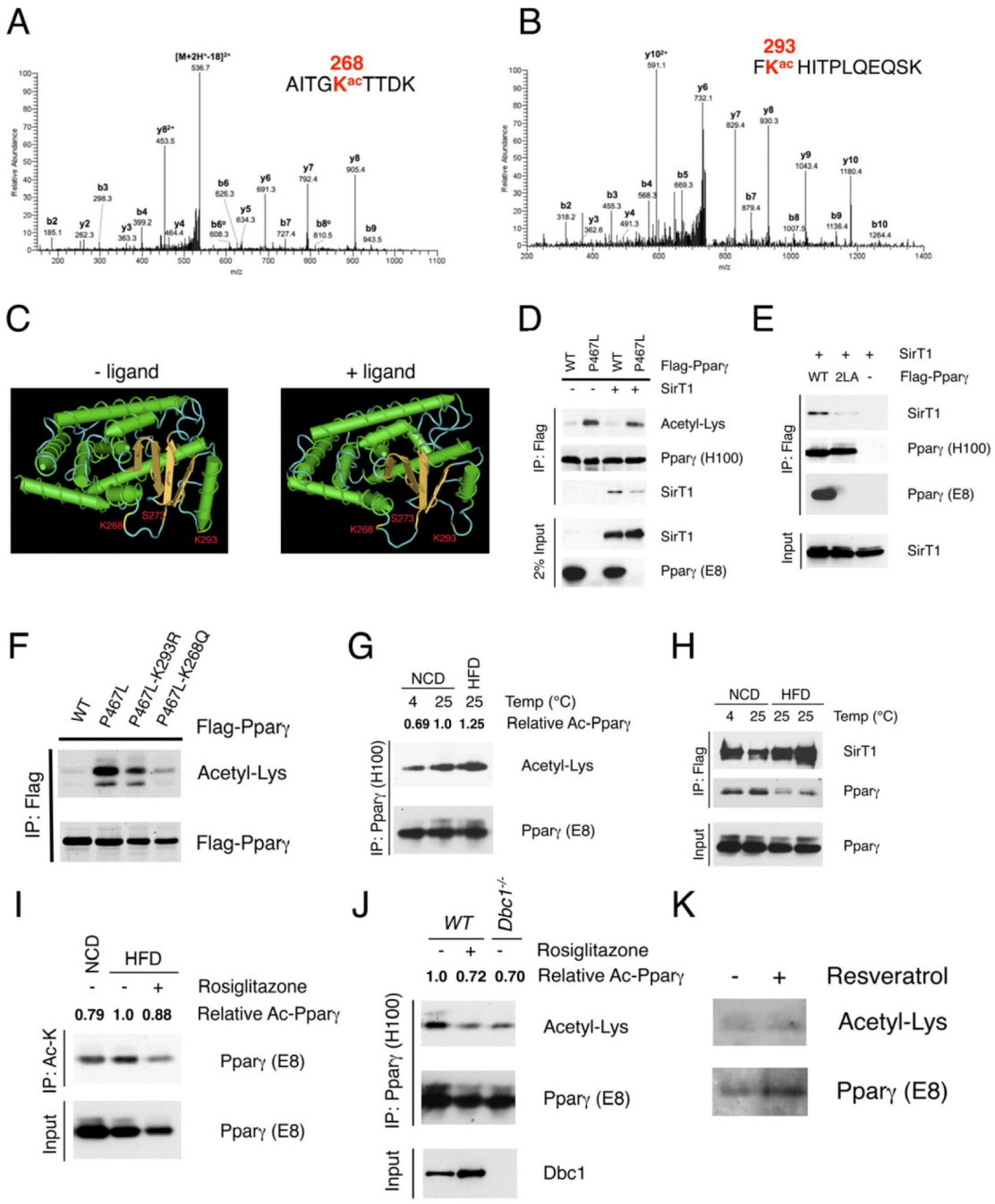

Figure 5. Identification of Pparγ Lys268 and Lys293 as SirT1 substrates

(A-B) Annotation of MS/MS spectra of acetylated peptides of Pparγ after trypsin digestion at Lys268 (A) and at Lys293 (B).

(C) 3-D model of liganded and unliganded Pparγ structure generated by NIH Cn3D software, localizing Lys268, Lys293 and Ser273 within helix 2-helix 2' region.

(D) Decreased SirT1 binding and increased acetylation of Pparγ P467L mutant. Co-IP of Flag-tagged WT or P467L mutant Pparγ with SirT1 in 293 cells. Pparγ (E8) antibody fails to recognize P467L mutant.

(E) Mutation of the LxxLL motif on helix 12 disrupts SirT1 binding. Co-IP of Flag-tagged WT or 2LA mutant Pparγ with SirT1 in 293 cells.

(F) Mutations of Lys268 or Lys293 decrease acetylation of P467L mutant Pparγ in 293 cells.
(G) Pparγ acetylation in pooled iWAT from 4-5 male mice exposed to 4 °C overnight or fed HFD for 16 weeks. We used 12 mg protein to immunoprecipitate Pparγ using antibody H100.
(H) Interaction of Pparγ with SirT1 in iWAT. Pooled iWAT from 3-5 male *SirBACO* mice exposed to 4 °C overnight or fed HFD for 16 weeks. We used 8 mg protein as in each lane to co-IP Flag-tagged SirT1.
(I) Pparγ acetylation in response to TZD following HFD. Male *WT* mice were fed HFD for 18 weeks and treated with rosiglitazone for 3 days. Pooled iWAT from 4 mice was lysed, and 12 mg protein was used in each lane to immunoprecipitate with acetyl-Lysine (Ac-K) antibody.
(J) Pparγ acetylation in response to TZD and deletion of Dbc1. Chow-fed male WT mice were treated with rosiglitazone for 3 days. 12 mg protein from pooled iWAT of 4 mice was used for IP with Pparγ antibody (H100).
(K) Pparγ acetylation in human adipose tissue in response to resveratrol. Human subcutaneous adipose fragments were treated with resveratrol (50 μM) for 12 hours. 1.2 mg protein was immunoprecipitated with Pparγ antibody (H100).
We estimated relative levels of Pparγ acetylation (Ac-Pparγ) using densitometry with NIH ImageJ software.
See also Figure S5.

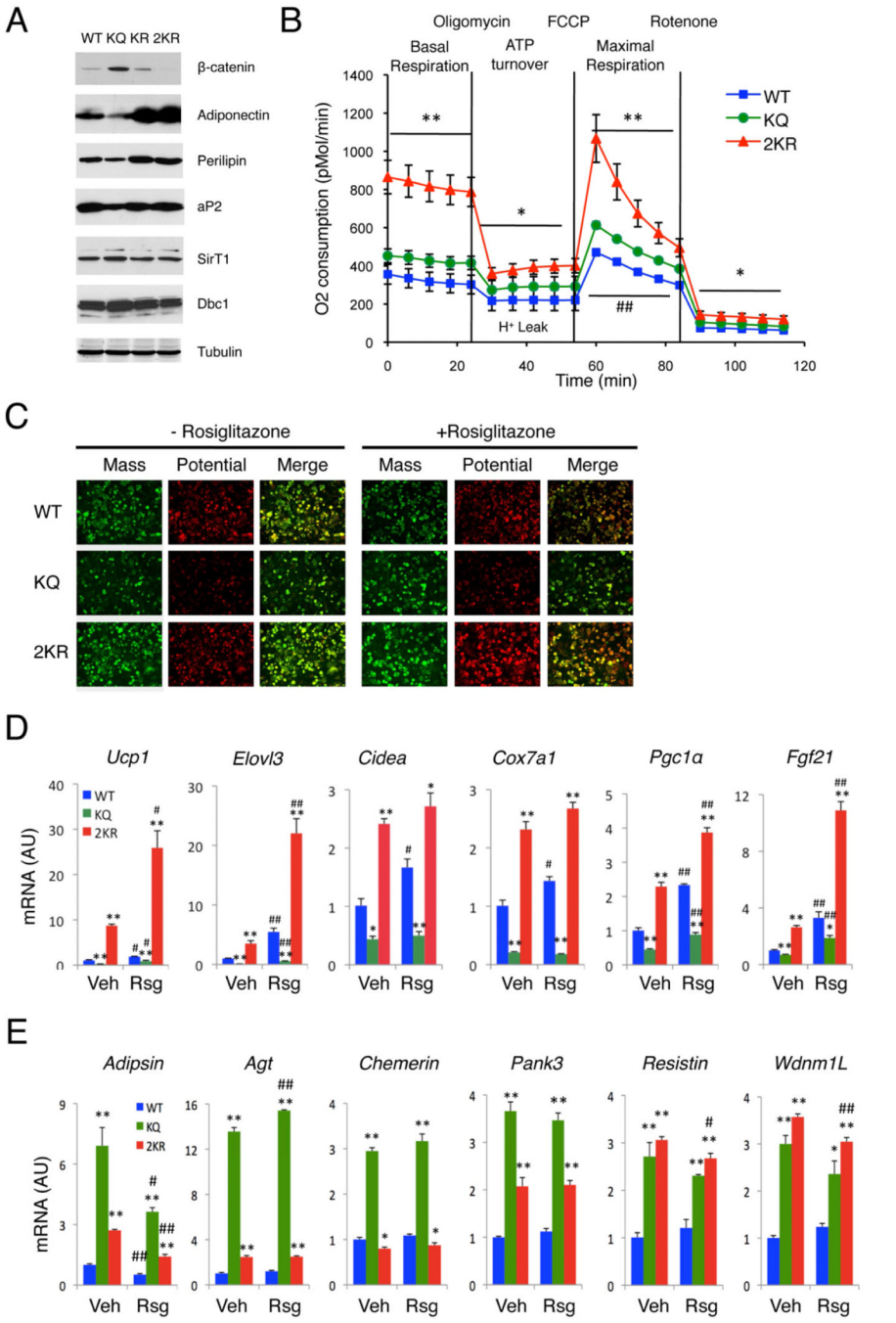

Figure 6. Deacetylation of Pparγ is required for its browning function

(A) Western blots analyses of Swiss 3T3 fibroblasts expressing WT, K293R (KR), K293Q (KQ) and K268R/K293R (2KR) Pparγ on day 6 of differentiation.

(B) Oxygen consumption rates (OCR) in fully differentiated cells (Day 8). *: $P<0.05$, **: $P<0.01$ for 2KR *vs.* WT cells; #: $P<0.05$, ##: $P<0.01$ for KQ *vs.* WT, n=6-7. The higher basal OCR in cells expressing the KQ mutant is likely due to increased cell number, owing to their shorter doubling time (Figure S6B).

(C) Mitochondrial mass (green) and membrane potential (red) on day 8 of differentiation.

(D-E) Brown gene (D) and white gene expression (E) on day 8 in cells treated with vehicle (Veh) or rosiglitazone (Rsg) overnight. *: $P<0.05$, **: $P<0.01$ *vs.* WT cells; #: $P<0.05$, ##: $P<0.01$ *vs.* untreated cells (n=3). Values are presented as means ± SEM.
See also Figure S6.

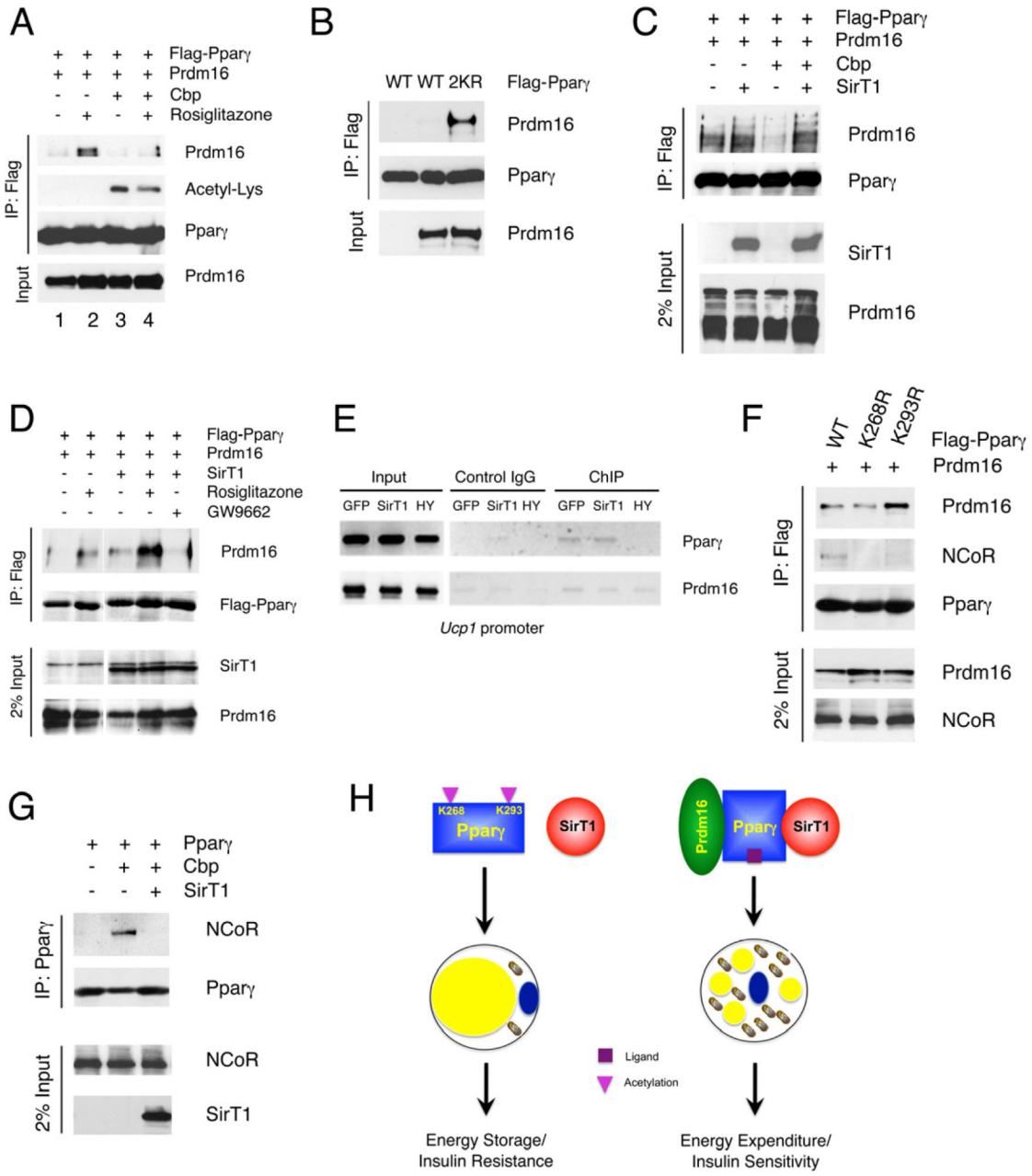

Figure 7. Deacetylation of Pparγ modulates the coactivator/corepressor exchange

(A) Pparγ interacts with Prdm16 in a ligand- and deacetylation-dependent manner. Co-IP of Flag-tagged Pparγ with Prdm16 in 293 cells, following Cbp transfection or rosiglitazone treatment.

(B) Acetylation-defective Pparγ increase binding of Prdm16. Co-IP of Flag-tagged Pparγ (WT) or 2KR mutant with Prdm16 in 293 cells.

(C) SirT1 promotes Pparγ interaction with Prdm16. Co-IP of Flag-tagged Pparγ with Prdm16 following transfection of Cbp and/or SirT1 in 293 cells.

(D) SirT1 mimics TZD to increase Pparγ interaction with Prdm16. Co-IP of Flag-tagged Pparγ with Prdm16 following overexpression of SirT1 and/or overnight treatments in 293 cells.

(E) ChIP analysis of Pparγ and Prdm16 binding to the *Ucp1* promoter in HIB-1B adipocytes expressing GFP, WT or H363Y (HY) mutant SirT1.
(F) Deacetylation of Pparγ Lys268 or Lys293 inhibits binding of NCoR. Co-IP of Flag-tagged Pparγ (WT), K268R or K293R mutants with exogenous Prdm16 and endogenous NCoR in 293 cells.
(G) Acetylation of Pparγ promotes binding of NCoR. Co-IP of Flag-tagged Pparγ with NCoR following transfection with SirT1 and Cbp in 293 cells.
(H) Model of SirT1-dependent Pparγ deacetylation in energy homeostasis and insulin sensitivity. When nutrients are available, SirT1 is inactive and Pparγ is acetylated on Lys268 and Lys293. This condition favors lipid storage. During energy deprivation, SirT1 becomes active and is recruited to Pparγ, possibly as a result of ligand-induced conformational changes, to deacetylate Lys268 and Lys293. In white adipocytes, the deacetylated Pparγ interacts with Prdm16 to promote thermogenesis (energy expenditure) and improve insulin sensitivity.
See also Figure S7.